Hindawi
International Journal of Antennas and Propagation
Volume 2022, Article ID 4553924, 8 pages
https://doi.org/10.1155/2022/4553924

Research Article

Conjoined, Two-Monopole Antenna Pair with Decoupling Inductor for Wi-Fi 6E Notebook Applications

Saou-Wen Su,[1] **Peng-Hao Juan**,[1] **and Fa-Shian Chang**[2]

[1]*Advanced EM & Wireless Communication R&D Center ASUSTek Computer Inc, Taipei 11259, Taiwan*
[2]*Department of Electronic Engineering, Cheng Shiu University, Kaohsiung 83347, Taiwan*

Correspondence should be addressed to Saou-Wen Su; saou-wen_su@asus.com

Received 4 July 2022; Revised 4 August 2022; Accepted 24 August 2022; Published 5 September 2022

Academic Editor: Mohammad Alibakhshikenari

A low-profile, conjoined and yet decoupled two-monopole design for Wi-Fi 6E notebook applications is presented. The single monopole antenna has a small size of 4 mm × 18.7 mm. The antenna is composed of a two-branched monopole with two shorting inductors for producing the 5 GHz (5150–5825 MHz) and 6 GHz (5925–7125 MHz) bands, and an inductor loaded at one branch end and connecting to a tuning portion for 2.4 GHz (2400–2484 MHz) operation. Two symmetrical monopoles are further conjoined by a chip inductor that connects the open ends of the tuning portions, forming a compact footprint of 4 mm × 38.4 mm for the two-notebook antenna design. With the use of the decoupling inductor and a proper two-monopole arrangement, acceptable isolation and a low envelop correlation coefficient (ECC) can be attained.

1. Introduction

In 2020, the Federal Communications Commission (FCC) opened up the additional spectrum in the 6 GHz band for unlicensed use [1]. This new 6 GHz (5925–7125 MHz) band consists of up to 1200 MHz bandwidth for providing faster wireless speeds and lower-latency services. Wireless devices able to operate in this new 6 GHz band are dubbed "Wi-Fi 6E" devices [2] to be differentiated from the present Wi-Fi 6 (IEEE 802.11ax) devices, which only cover the 2.4 GHz (2400–2484 MHz) and 5 GHz (5150–5825 MHz) wireless local area network (WLAN) bands. With the biggest upgrade in 20 years, multi-Gbps connections are foreseen in the immediate future and are on par with fifth-generation (5G) communications [3].

For the notebook industry, it has become very much in demand that the antennas can function in the 2.4/5/6 GHz multiple bands to meet Wi-Fi 6E specifications. A few new antenna designs have recently been reported as Wi-Fi 6E-ready antennas [4–6]. These antennas not only need to cover the 5150–7125 MHz range in the upper band but keep a low profile to fit into the narrow-bezel width (typically less than 5 mm [7]) of the notebook display. Additionally, to save precious design space within devices, two antenna elements are required to be placed in the vicinity, in which antenna separation is usually less than a quarter wavelength in free space [8].

However, closely-packed antenna elements in the same frequency bands usually suffer from high mutual coupling, which degrades the RF sensitivity of the multiantenna system. Numerous decoupling methods have been studied in the literature [9–25]. One often-seen decoupling method is to introduce an additional coupling path between the antennas to counter the original coupling by adding the resonant structure [9–11].

For the design without any decoupling resonant structure [12–14], the capacitive loads [12, 13] are tapped on the shorting strips of the inverted-F antennas (IFAs); however, the separation distance of 9 mm in [12] is too large for achieving only the 2.4 GHz band. Also, the addition of the branch strips to the original IFAs in [14] for inductive and capacitive coupling cancellation increases the total antenna design size, which is not favorable to notebook antenna design. Another method without introducing the resonant structure between the antennas is to design the decoupling network on the antenna/system ground plane [15, 16]. The

methodology is usually involved with complex formulas, scattering matrices, transmission line theory, etc. The main concern with the decoupling network is that it occupies too much board space for practical applications in mobile phones and notebook computers.

For the antennas without any separation, the mode-cancellation technique has been introduced to the conjoined antennas [6, 17] and the antenna pairs reported in [18–22]. These works mainly utilize two resonant modes of similar magnitudes but 180-degree out-of-phase currents on the coupled antenna or shared radiator. The decoupling analysis using the common and differential modes of cancellation is popularly practiced in these studies [19, 21, 22]. Another simple yet effective method is to directly connect two antennas with a decoupling inductor [23–25]. The location of the inductor is loaded between the open ends of the antennas [23, 24] or around [26]. In this case, the chip inductor and antenna spacing (considered a distributed capacitor) form a band-stop circuit to reduce the coupling between the antennas. In addition, depending on the decoupling of which antenna frequency bands, the lower the decoupled antenna frequencies, the larger the inductance required.

In this paper, based on the previous single-antenna design in [4] and the use of the decoupling chip inductor [23–25], a compact and yet decoupled two-monopole design for Wi-Fi 6E notebooks is proposed. The two identical branched monopoles are conjoined with the 5/6 GHz strips set face-to-face and connected by a decoupling inductor. The design occupies a compact footprint of 4 mm × 38.4 mm. Acceptable low coupling with S_{21} <– 13 dB and good radiation performance with low envelop correlation coefficient (ECC) over the 2.4 and 5/6 GHz bands are also attained. The proposed prototype was analyzed in simulation and verified by measurement. The design details are described and discussed in the following sections.

2. Proposed, Conjoined Monopole Antennas

Figure 1(a) shows the geometry of the proposed conjoined monopoles located above the display ground plate of size 182 mm × 315 mm for 14-inch notebooks. The design is constructed on a 0.8-mm-thin, FR4 substrate ($\varepsilon_r = 4.4$ and $\tan\delta = 0.02$) of size 4 mm × 38.4 mm and placed 15 mm from the top-right point of the ground plate. This 15 mm keep-out zone, not for antenna placement, is designated for mechanical assembly structures. A prototype photo is presented in Figure 1(b), in which a large, 70 mm × 50 mm copper tape was used to ground the design and also helped alleviate the unwanted leakage currents of the antenna cables during measurement [26].

The proposed design is composed of two identical monopoles (Ant1 and Ant2) arranged face-to-face with a 1 mm spacing between them. The single monopole (Ant1) comprises a two-branched monopole with two shorting inductors ($L1$, $L2$) and a chip inductor ($L3$) loaded to the end of the monopole and further connecting to a tuning portion. The resonant paths of 8.9–9 mm from the feed port to the open ends with similar lengths (4.9–5 mm) of the two radiating branches correspond to a 0.18-free-space wavelength at 6 GHz. Additionally, two inductors ($L1$, $L2$), located 1 mm to the port, short-circuit the monopole for better matching over the 5150–7125 MHz frequency range.

A third chip inductor ($L3$) of large inductance, which is loaded at one end of the monopole, interconnects the monopole and the tuning portion. This inductor provides an extra, lower-band resonant path for 2.4 GHz operation without much affecting the 5/6 GHz bands. In this case, the monopole can be fine-tuned using this tuning portion to cover the 2400–2484 MHz frequency range. The preferred parameters are obtained with the aid of Ansys HFSS, an electromagnetic solver [27].

A chip inductor ($L7$) for antenna decoupling is further employed to conjoin the two monopoles (Ant1 and Ant2). Because of the small spacing (1 mm) between the monopoles, large capacitive coupling occurs, similar to a distributed capacitor. It is known that the currents are at their minimum at the end of the 0.25-wavelength monopole. When the chip inductor is loaded into the current-null region, the 0.25-wavelength resonant mode is not much affected. In this case, the chip inductor provides an additional current path, whose length is determined by the inductor values. The loaded inductor and the spacing between the two-monopole ends form an L/C parallel band-stop circuit. The band-stop frequencies can be adjusted by the inductance with fixed capacitance (spacing between the open ends). Accordingly, the antenna port-to-port signals are filtered, resulting in lower coupling between Ant1 and Ant2.

In addition, there exist two possible arrangements for Ant1 and Ant2, namely the 5/6 GHz resonant strips face-to-face and 2.4 GHz resonant strips (tuning portions) face-to-face [see insets in Figures 2(a) and 2(b)]. The simulated reflection and transmission coefficients for the two cases are studied in Figure 3. The dimensions of these cases are all the same, but the inductance of the $L7$ varies depending on decoupling which frequency bands. Both cases show a good impedance bandwidth with reflection coefficients (S_{11} for Ant1, S_{22} for Ant2) below −7.3 dB, which is acceptable for industrial notebook-antenna designs. However, the transmission coefficient (S_{21} between two antenna ports) for the reference [see Figure 2(b)] in the 5/6 GHz bands is lower than −9 dB only, compared with that for the proposed design in Figure 2(b). In fact, the proposed arrangement with 5/6 GHz resonant strips face-to-face leads to a lower transmission coefficient (lower than −13 dB) in all the bands of interest. It is noteworthy that a much larger inductance is required to decouple the lower band ($L7$ = 91 nH for the 2.4 GHz band) [24] than the upper band ($L7$ = 8.2 nH for the 5/6 GHz bands).

3. Results and Discussions

Figure 3(a) shows the measured and simulated reflection and transmission coefficients for the proposed conjoined monopoles. The measured curves are plotted in the dashed lines. The targeted 2.4, 5, and new 6 GHz bands are all marked by the shaded frequency ranges. Two 130 mm coaxial cables were used for feeding the monopoles through a gap of 1 mm [see Figure 1(b)]. The experimental results generally agree with the simulation. The discrepancies are owing to the fabrication tolerance and the cables in the

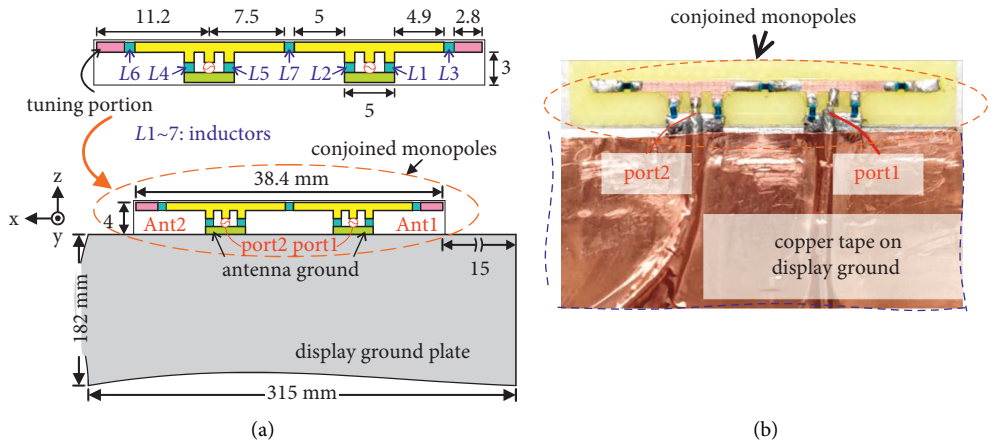

Figure 1: (a) Geometry of the conjoined MIMO antennas for Wi-Fi 6E notebooks. (b) Photo of a fabricated prototype.

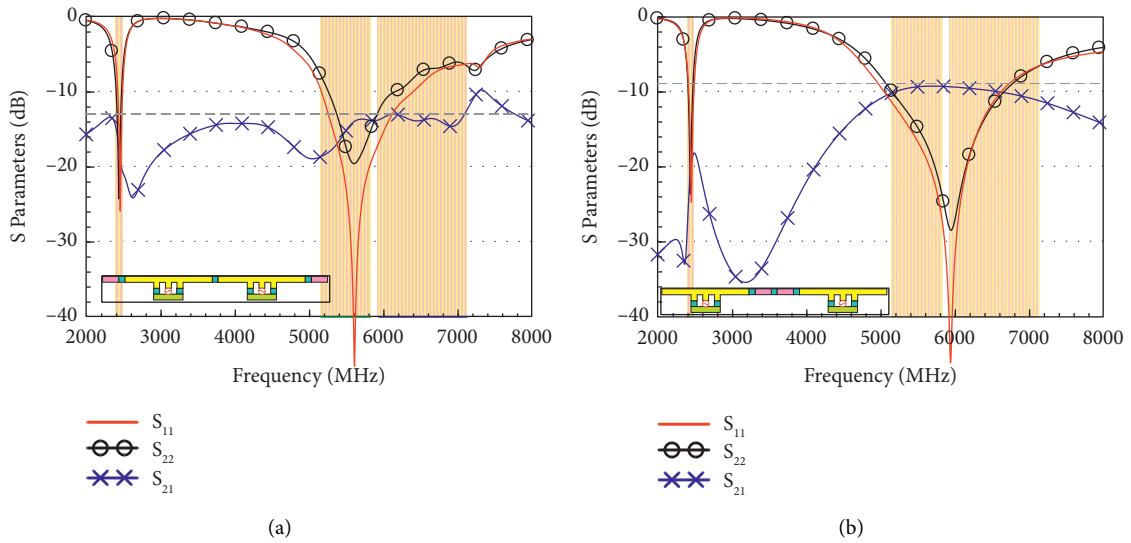

Figure 2: Simulated reflection and transmission coefficients S11 for Ant1, S22 for Ant2, and S21 between two ports for (a) the proposed (5/6 GHz resonant strips face-to-face) with $L7 = 8.2$ nH and (b) the reference (2.4 GHz resonant strips face-to-face) with $L7 = 91$ nH.

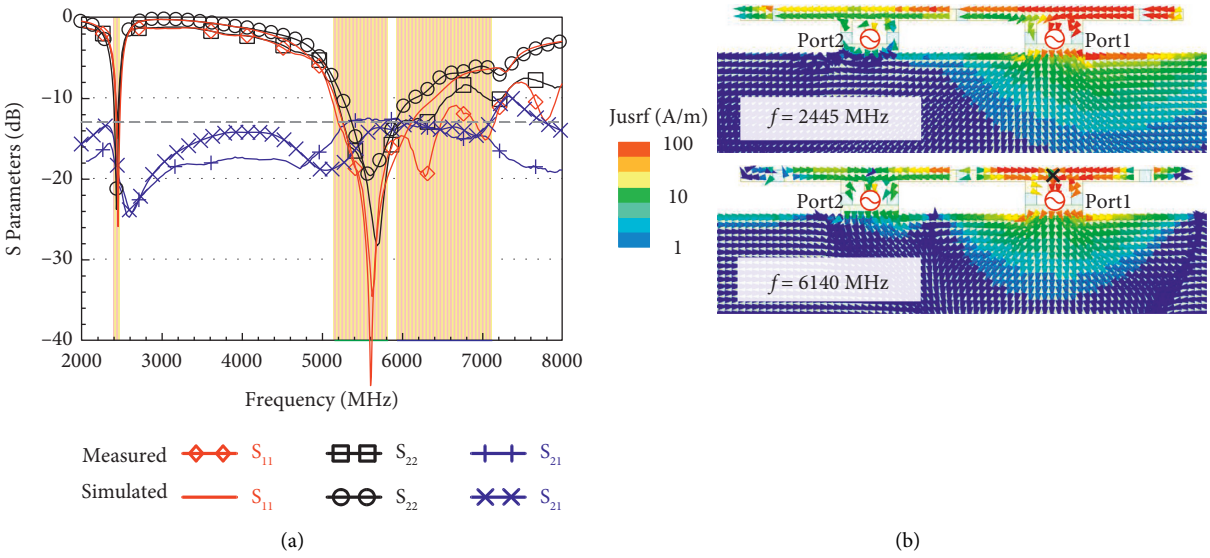

Figure 3: (a) Measured and simulated reflection and transmission coefficients; $L1$, $L2$, $L4$, $L5 = 5.6$ nH, $L3 = L6 = 18$ nH, $L7 = 8.2$ nH. (b) The simulated surface current distribution of Ant1 excited at 2445 and 6140 MHz.

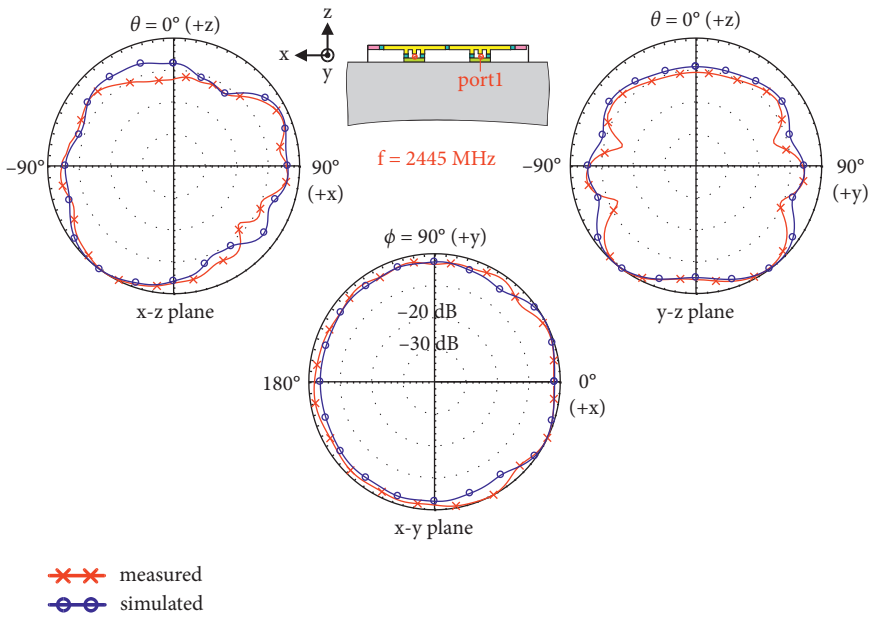

(a)

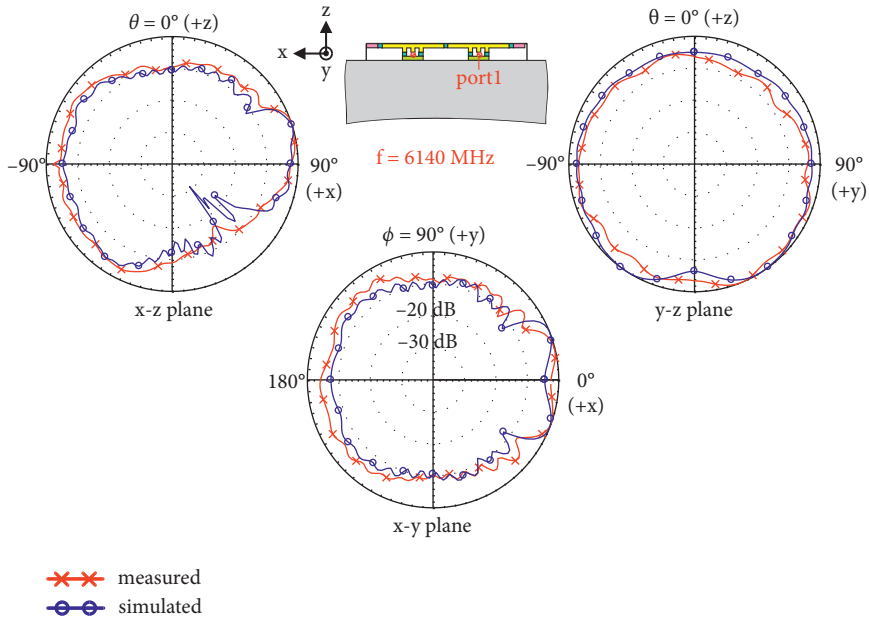

(b)

Figure 4: Continued.

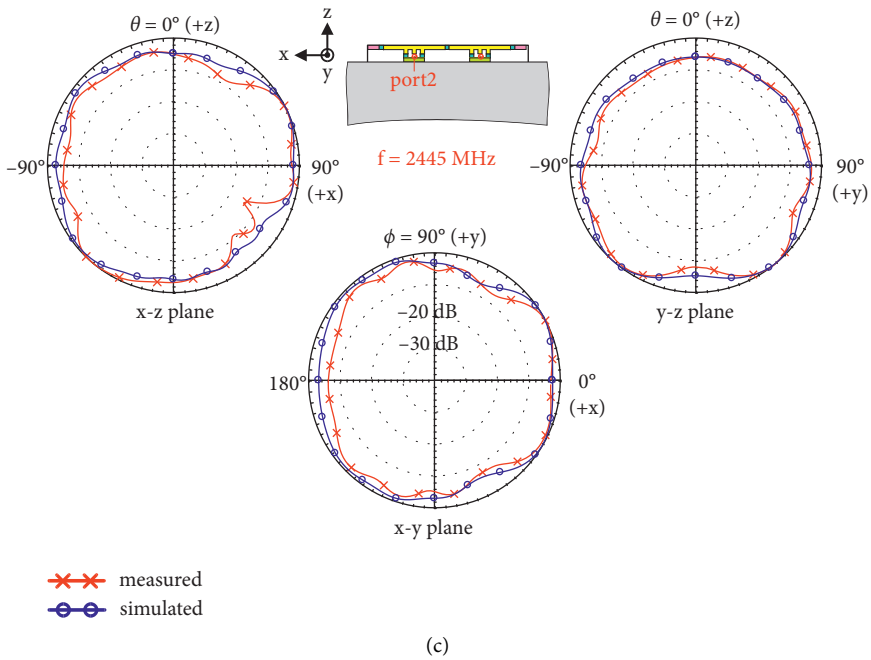

(c)

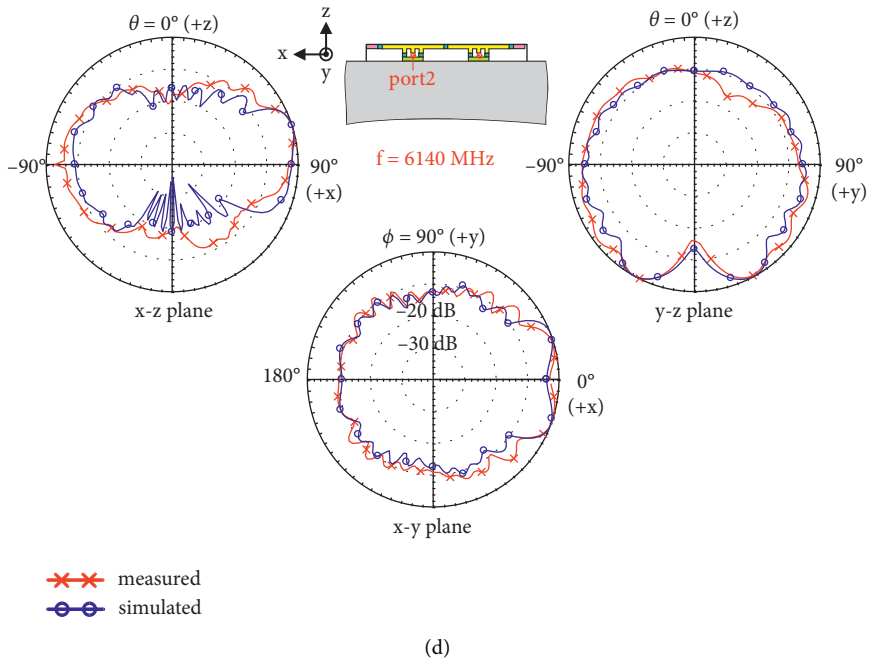

(d)

Figure 4: Measured 2-D radiation patterns (E-total) at 2445 and 6140 MHz. (a) Ant1. (b) Ant2.

measurement. With an impedance better than −7.3 dB, the reflection coefficients cover all frequency bands of interest for 2.4/5/6 GHz operation. The transmission coefficients are lower than −16 and −13 dB in the 2.4 and 5/6 GHz bands.

Figure 3(b) presents the simulated current distribution of Ant1 excited at 2445 and 6140 MHz. For the lower-band excitation at 2445 MHz, stronger surface currents are found on Ant1, the right side of the conjoined design, and also the portion below the 2.4 GHz strip (tuning portion) on the display ground (corresponding image currents). As for the upper band at 6140 MHz, larger currents are distributed on the two-branch monopole of An1 with fewer currents on the tuning portion. The corresponding image currents are also seen right below the two-branch monopole. These properties suggest that the antenna coupling between the two conjoined monopoles has been alleviated by the use of the decoupling chip inductor ($L7$).

The radiation characteristics were verified at the MVG SATIMO SG 24, which has amultiprobe array and tests the spectrum up to 10 GHz [28]. Figures 4(a)–4(d) plots the measured and simulated 2-D radiation patterns in the E-total field at 2445 and 6140 MHz, the central frequencies, respectively, for the 2.4 and 5/6 GHz bands. From our empirical test results on actual notebooks, the E-total gain patterns, instead of separate polarization in $E\theta$ and $E\varphi$ fields,

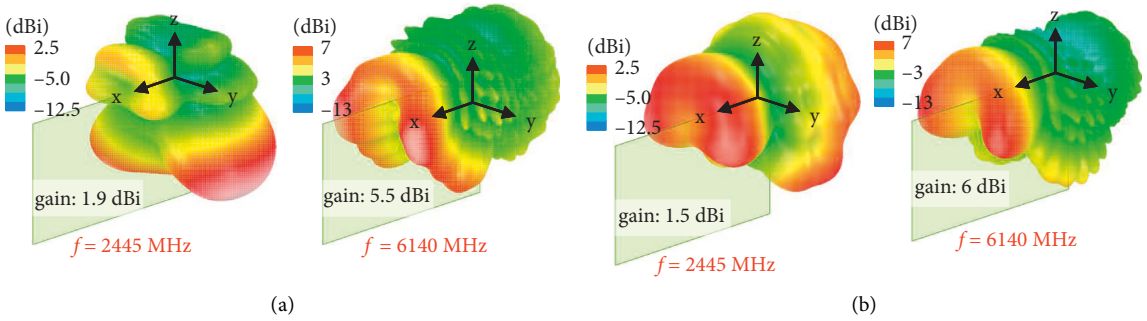

Figure 5: Simulated 3-D radiation patterns for the proposed design. (a) Ant1. (b) Ant2.

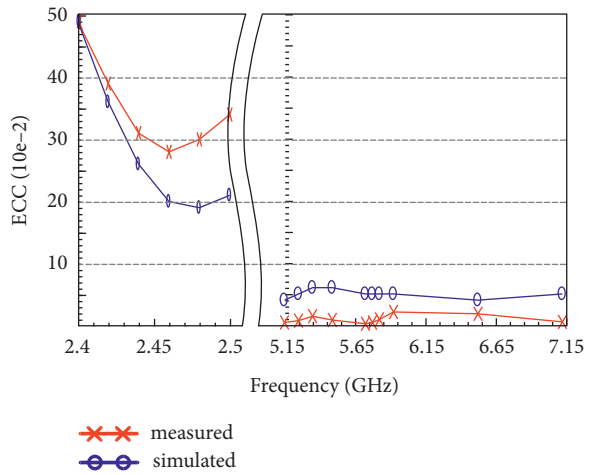

Figure 6: Calculated ECC using the radiation patterns of Ant1 and Ant2.

Table 1: Comparison of the proposed design and other cited works [9–25]. λ is the free-space wavelength at the lowest frequency in the designed frequency band. Isolation is the largest value (worst case) over all the obtained bands.

Ref.	Frequency band (GHz)	Size (λ)	Spacing (mm)	Isolation (dB)	Decoupling method	Applications
[9]	2.4/5	0.06×0.37	14.4 (0.11–λ)	15	Resonant structure	N.A.
[10]	2.4/5	0.04×0.32	1.6 (0.013–λ)	15	Resonant structure	Notebook
[11]	2.4/5	0.04×0.30	2 (0.016–λ)	16	Resonant structure	Notebook
[12]	2.4	0.08×0.34	9 (0.072–λ)	16	Two-port S matrix	Phone
[13]	2.11–2.17	0.07×0.38	6.6 (0.043–λ)	17	Multi-port S matrix	Phone
[14]	3.3–3.8	0.15×0.46	2 (0.033–λ)	20	Equivalent circuit model for LC couplings	Phone
[15]	1.88–1.92	0.13×0.19	4.6 (0.029–λ)	25	Decoupling network	N.A.
[16]	2.4/5	0.09×0.37	4 (0.032–λ)	21	Decoupling matching network	N.A.
[17]	2.4.5	0.04×0.32	0	16	Dipole/monopole mode cancellation	Notebook
[18]	3.3–5.0	0.05×0.38	0	16	1.0–/1.5–λ loop mode cancellation	Notebook
[19]	3.4–4.2	0.09×0.34	0	10	CM/DM cancellation	Phone
[20]	3.3–3.5	0.05×0.38	0	13	0.5–/1.0–λ loop mode cancellation	Notebook
[21]	3.4–3.6	0.07×0.18	0	10	CM/DM cancellation	Phone
[22]	5/6	$0.28 \times 0.40^*$	0	20	CM/DM cancellation	N.A.
[23]	3.4–3.8	0.05×0.23	1 (0.012–λ)	16	Parallel L/C band-stop circuit	tablet
[24]	2.4/5	0.04×0.33	1 (0.008–λ)	17	Parallel L/C band-stop circuit	Notebook
[25]	3.4–3.6	0.04×0.46	1 (0.012–λ)	11	Parallel L/C band-stop circuit	Phone
Proposed	2.4/5/6	0.03×0.32	1 (0.008–λ)	13	Parallel L/C band-stop circuit	Notebook

N. A, not available. * patch antenna with 4 mm air spacing above the ground plane.

can determine the data throughput performance. It is because, in the real multipath environment, both polarization coexist. The omnidirectional and near-omnidirectional patterns can be observed in the x-y and y-z planes in the 2.4 GHz band. For 5/6 GHz operation, less radiation is seen in the elevation planes toward the $+z$ direction.

Figures 5(a) and 5(b) present the corresponding, 3-D radiation patterns at 2445 and 6140 MHz for Ant1 and Ant2.

The 3-D radiation characteristics correspond to the 2-D patterns in each plane as studied in Figure 4. The antenna efficiency and peak antenna gain were measured (figures not presented for brevity), and the antenna mismatch and cable loss were all taken into account in the measurement. For Ant1 over the 2.4 and 5/6 GHz bands, the peak gain is in the range of 1.4–1.7 and 2.2–5.3 dBi with an antenna efficiency larger than 27% and 59%, respectively. As for Ant2, the gain is about 1.0–1.2 and 2.8–6.1 dBi with efficiency greater than 27% and 56% in the lower and upper bands.

The measured and simulated envelope correlation coefficients (ECC) between two monopoles are shown in Figure 6. This figure of merit is based on the calculations of the two complex far fields [29] in the uniform multipath surroundings [30] and reflects the similarity between the radiation characteristics of the two antennas. Results for low ECC less than 0.49 and 0.02, respectively, over the 2.4 and 5/6 GHz bands are obtained in this work. Notice that for mobile devices, an ECC less than 0.5 [31, 32] is regarded as a low value for good antenna diversity gain.

Finally, a comparison table (see Table 1) for the proposed work and other cited papers is also provided in this section. Notice that isolation is a positive value and the negative value of the transmission coefficient [30]. Several key aspects are tabulated, including the designed frequency band, antenna size and spacing, isolation, decoupling method, and wireless device applications. Notice that for a fair comparison, the electrical length in λ, which represents the free-space wavelength at the lowest frequency in the designed band (see column title 2 in Table 1), is used for antenna size and spacing. Compared with the same WLAN designs [9–12, 16, 17, 22, 24], the proposed antenna can cover the new 6 GHz band for 2.4/5/6 GHz Wi-Fi 6E operation and also offers a smaller antenna size. Moreover, this work does not require additional space between the antennas [9–16] or any board space on the antenna/system ground [15, 16]. Although a 1 mm antenna spacing is needed for the chip inductor in this design, the design footprint is smaller than those studies with no separation between the antennas [17–22]. As far as the authors are concerned, the proposed design has the lowest profile (0.03–λ) and yet covers more antenna bands (2.4/5/6 GHz) among WLAN notebook antennas and others shown in Table 1.

4. Conclusion

A printed, conjoined two-monopole design covering the present 2.4/5 GHz and the new 6 GHz WLAN bands for narrow-bezel, Wi-Fi 6E notebook applications has been introduced. The two-antenna footprint occupies a compact size of 4 mm × 38.4 mm with a low profile of about 0.03–λ at 2.4 GHz. The design uses two two-branched monopoles with shorting inductors for producing the 5150–7125 MHz wideband range. The lower-band resonance for 2.4 GHz operation is obtained by the low-pass, matching inductor that connects to the tuning portion. The two monopoles are further conjoined with the 5/6 GHz strips set face-to-face and connected by a decoupling inductor. Acceptable low coupling with S_{21} <− 13 dB and good radiation performance with low ECC over the 2.4 and 5/6 GHz bands are also attained.

Data Availability

The single antenna [2] used to support the findings of this study is included in the article [2] 10.1109/APS/URSI47566.2021.9703930.

Conflicts of Interest

The authors declare that there are no conflicts of interest.

References

[1] Federal Communications Commission, "FCC Opens 6 GHz Band to Wi-Fi and Other Unlicensed Uses," 2020, https://www.fcc.gov/document/fcc-opens-6-ghz-band-%20wi-fi-and-other-unlicensed-uses-0.

[2] Wi-Fi Alliance, "Wi-Fi Alliance brings Wi-Fi 6 into 6 GHz," 2020, https://www.wi-fi.org/%20news-events/newsroom/wi-fi-alliance-brings-wi-fi-6-into-6-ghz.

[3] Wireless Broadband Alliance, "WBA's First Phase of Wi-Fi 6E Trials Shows the Massive Potential of Wi-Fi in the 6GHz Band," 2020, https://www.realwire.com/%20releases/WBAs-First-Phase-of-Wi-Fi-6E-Trials-Shows-the-Massive-Potential-of-Wi-Fi.

[4] S. W. Su, "Compact, small, chip-inductor-loaded Wi-Fi 6E monopole antenna," in *Proceedings of the 2021 IEEE International Symposium on Antennas and Propagation and USNC-URSI Radio Science Meeting (APS/URSI)*, Singapore, December 2021.

[5] S. W. Su and C. C. Wan, "Asymmetrical, self-isolated laptop antenna in the 2.4/5/6 GHz Wi-Fi 6E bands," in *Proceedings of the 2021 International Symposium on Antennas and Propagation (ISAP)*, Taipei, Taiwan, October 2021.

[6] S. W. Su, D. P. Yusuf, and F. H. Chu, "Conjoined, Wi-Fi 6E MIMO antennas for laptops," in *Proceedings of the 2021 International Symposium on Antennas and Propagation (ISAP)*, vol. 1-2, Taipei, Taiwan, Taipei, Taiwan, October 2021.

[7] S. W. Su, C. T. Lee, and S. C. Chen, "Compact, printed, tri-band loop antenna with capacitively-driven feed and end-loaded inductor for notebook computer applications," *IEEE Access*, vol. 6, pp. 6692–6699, 2018.

[8] A. C. K. Mak, C. R. Rowell, and R. D. Murch, "Isolation enhancement between two closely packed antennas," *IEEE Transactions on Antennas and Propagation*, vol. 56, no. 11, pp. 3411–3419, 2008.

[9] J. Y. Deng, J. Y. Li, L. Zhao, and L. X. Guo, "A dual-band inverted-F MIMO antenna with enhanced isolation for WLAN applications," *IEEE Antennas and Wireless Propagation Letters*, vol. 16, pp. 2270–2273, 2017.

[10] S. W. Su and Y. W. Hsiao, "Small-sized, decoupled two-monopole antenna system using the same monopole as decoupling structure," *Microwave and Optical Technology Letters*, vol. 61, no. 9, pp. 2049–2055, 2019.

[11] S. W. Su, C. T. Lee, and Y. W. Hsiao, "Compact two-inverted-F-antenna system with highly integrated π -shaped decoupling structure," *IEEE Transactions on Antennas and Propagation*, vol. 67, no. 9, pp. 6182–6186, 2019.

[12] J. Sui and K. L. Wu, "Self-curing decoupling technique for two inverted-F antennas with capacitive loads," *IEEE Transactions on Antennas and Propagation*, vol. 66, no. 3, pp. 1093–1101, 2018.

[13] J. Sui, Y. Dou, X. Mei, and K. L. Wu, "Self-curing decoupling technique for MIMO antenna arrays in mobile terminals," *IEEE Transactions on Antennas and Propagation*, vol. 68, no. 2, pp. 838–849, 2020.

[14] J. Sui and K. L. Wu, "A self-decoupled antenna array using inductive and capacitive couplings cancellation," *IEEE Transactions on Antennas and Propagation*, vol. 68, no. 7, pp. 5289–5296, 2020.

[15] M. Li, L. Jiang, and K. L. Yeung, "A novel wideband decoupling network for two antennas based on the wilkinson power divider," *IEEE Transactions on Antennas and Propagation*, vol. 68, no. 7, pp. 5082–5094, 2020.

[16] M. Li, Y. Zhang, D. Wu, K. L. Yeung, L. Jiang, and R. Murch, "Decoupling and matching network for dual-band MIMO antennas," *IEEE Transactions on Antennas and Propagation*, vol. 70, no. 3, pp. 1764–1775, 2022.

[17] C. C. Wan and S. W. Su, "Conjoined, 2.4/5-GHz WLAN two-monopole system decoupled using mode-controlled capacitor for notebook computers," *Progress in Electromagnetics Research M*, vol. 87, pp. 1–10, 2019.

[18] W. H. Chang, S. W. Su, and B. C. Tseng, "Self-decoupled, 5G NR77/78/79 two-antenna system for notebook computers," in *Proceedings of the 2019 Electrical Design of Advanced Packaging and Systems (EDAPS)*, Kaohsiung, Taiwan, December 2019.

[19] L. Sun, Y. Li, Z. Zhang, and H. Wang, "Self-decoupled MIMO antenna pair with shared radiator for 5G smartphones," *IEEE Transactions on Antennas and Propagation*, vol. 68, no. 5, pp. 3423–3432, 2020.

[20] C. T. Lee and S. W. Su, "Decoupled multi-input multi-output antennas with a common dipole for wideband 5G laptop computers," *Microwave and Optical Technology Letters*, vol. 63, no. 4, pp. 1286–1293, 2020.

[21] Y. Ye, X. Zhao, and J. Wang, "Compact high-isolated MIMO antenna module with chip capacitive decoupler for 5G mobile terminals," *IEEE Antennas and Wireless Propagation Letters*, vol. 21, no. 5, pp. 928–932, 2022.

[22] W. Zhang, Y. Li, K. Wei, and Z. Zhang, "A two-port microstrip antenna with high isolation for Wi-Fi 6 and Wi-Fi 6E applications," *IEEE Transactions on Antennas and Propagation*, vol. 70, no. 7, pp. 5227–5234, 2022.

[23] K. L. Wong and L. Y. Chen, "Dual-inverted-F antenna with a decoupling chip inductor for the 3.6 GHz LTE operation in the tablet computer," *Microwave and Optical Technology Letters*, vol. 57, no. 9, pp. 2189–2194, 2015.

[24] S. W. Su, C. T. Lee, and S. C. Chen, "Very-low-profile, triband, two-antenna system for WLAN notebook computers," *IEEE Antennas and Wireless Propagation Letters*, vol. 17, no. 9, pp. 1626–1629, 2018.

[25] C. Deng, D. Liu, and X. Lv, "Tightly-arranged four-element MIMO antennas for 5G mobile terminals," *IEEE Transactions on Antennas and Propagation*, vol. 67, no. 10, pp. 6353–6361, 2019.

[26] B. Drozd and W. T. Joines, "Comparison of coaxial dipole antennas for applications in the near-field regions," *Microwave Journal*, vol. 47, no. 5, pp. 160–176, 2004.

[27] H. F. S. S. Ansys, "Ansys Inc," http://www.ansys.com/Products/Electronics/ANSYS-HFSS.

[28] SG 24-S, "MVG," 2020, https://www.mvg-world.com/en/products/antenna-measurement/%20multi-probe-systems/sg-24.

[29] S. Blanch, J. Romeu, and I. Corbella, "Exact representation of antenna system diversity performance from input parameter description," *Electronics Letters*, vol. 39, no. 9, pp. 705–707, 2003.

[30] M. S. Sharawi, "Printed multi-band MIMO antenna systems and their performance metrics [wireless corner]," *IEEE Antennas and Propagation Magazine*, vol. 55, no. 5, pp. 218–232, 2013.

[31] R. G. Vaughan and J. B. Andersen, "Antenna diversity in mobile communications," *IEEE Transactions on Vehicular Technology*, vol. 36, no. 4, pp. 149–172, 1987.

[32] K. R. Jha and S. K. Sharma, "Combination of MIMO antennas for handheld devices [wireless corner]," *IEEE Antennas and Propagation Magazine*, vol. 60, no. 1, pp. 118–131, 2018.